# Synthetic Saponite Clays as Additives for Reducing Aging Effects in PIM1 Membranes

# Synthetic saponite clays as additives for reducing aging effects in PIM1 membranes

Federico Begni[a], Geo Paul[a], Elsa Lasseuguette[b], Enzo Mangano[b], Chiara Bisio[a,c*], Maria-Chiara Ferrari[b*], Giorgio Gatti[a]

[a]*Dipartimento di Scienze e Innovazione Tecnologica, Università degli Studi del Piemonte Orientale" Amedeo Avogadro", Viale Teresa Michel 11, 15121-Alessandria (Italy);*

[b] *School of Engineering, University of Edinburgh, Robert Stevenson Road, EH9 3FB, Edinburgh, UK*

[c]*CNR-SCITEC Istituto di Scienze e Tecnologie Chimiche "G. Natta", Via C. Golgi 19, 20133-Milano (Italy).*

*Corresponding Authors:* chiara.bisio@uniupo.it; m.ferrari@ed.ac.uk

## ABSTRACT

Polymers of Intrinsic Microporosity represent one of the most promising polymeric materials for gas separation applications. Their very rigid and contorted backbone induces unusually high free volumes and high internal surface area, with high gas permeabilities and moderate ideal selectivity, especially for $O_2/N_2$, $CO_2/N_2$ pairs with values lying above the Robeson's upper bound. However, the high FFV of PIM1 tends to be shortlived, soon collapsing to leave fewer transport pathways and reduce gas permeability. One way to tackle this problem is the addition of fillers within the polymeric matrix. Here we report the use of synthetic clays named saponites as fillers, to slow down the physical aging of PIM1 membranes. Mixed Matrix Membranes (MMMs) based on two different saponites samples (one completely inorganic and one functionalized with a surfactant) have been obtained and their permeation performances have been studied in the course of one year in order to explore physical aging effects over time. Without filler, PIM1 exhibits the classical aging behaviour of polymers of intrinsic microporosity, namely a progressive decline in gas permeation. On the contrary, with saponites, MMMs present a plateau after one week within the aging showing that the fillers slow down the aging of PIM1 membranes in the long term. After one year of aging, the total reduction for $CO_2$ permeability for native PIM1 was 80% whereas for the MMMs it was 53% and 59% for the inorganic and the functionalized saponite respectively. Interactions between

the fillers and the polymeric matrix in addition to aging effects have been also monitored through ss-NMR spectroscopy. The $^{13}C$ spin–lattice relaxation time (T1) measurements reveal that PIM1 chains intercalation between T-O-T lamellar sheets could be one of the mechanisms responsible of PIM1 slowing down aging. Chains confinement between lamellar sheets could play a significant role in reducing chains densification, while maintaining small free volumes.

***Keywords:*** *PIM1, saponite, permeation, aging-effects, ss-NMR, relaxation times*

## INTRODUCTION

Gas separation and purification through membrane technology has become a promising candidate as alternative way to $CO_2$ chemical absorption for carbon capture applications[1]. Even though amine-based absorption is still the most mature method for the capturing of $CO_2$, from both natural and flue gas[2], it presents some serious drawbacks. Plant corrosion is usually reported as one of the major issues associated with this type of technology, along with a substantial energetic demand due to regeneration of the liquid phase solvent (around 3.5 GJ per ton of $CO_2$) and environmental concerns on the release of toxic species[3]. Membrane gas separation is considered a more environment friendly alternative that exploits the intrinsic ability of permeable materials to selectively separate single components from a gas mixture. The lower costs due to lower energy requirements and the ease of operation give membranes an advantage over other separation technologies[4]. In this respect, polymeric membranes are particularly interesting because of the incredibly diverse landscape of possible synthetic pathways for new materials in combination to simple and relatively cheap production which can result in a more advantageous scale up for industrial application[2]. Polymers of Intrinsic Microporosity (PIM) recently have become the most studied polymeric materials for membrane applications, starting from the first one synthesized, PIM1[5,6]; PIM1 is especially suitable to be processed as a gas separation membrane thanks to its long and flexible polymeric chains which pack themselves inefficiently[7], thus causing the generation of internal free volume and eventually, diffusion pathways for gas molecules. However, chain linearity and consequently easy processability, come with the cost of fast physical aging[8]. Aging is a thermodynamic driven process and it is manifested as the tendency of the polymeric chains to collapse, thus reducing free volume and consequently diffusion pathways and is particularly pronounced in

high free volume polymers[9,10].One way to tackle this problem is the addition of fillers within the polymeric matrix. This strategy has been reported for a wide number of fillers,[10-15] in particular the addition of porous polymers (Porous Aromatic Frameworks, PAFs) as fillers has proven to be very effective in reducing physical aging[15,16], however their high cost of production prevents an industrial scale implementation. Up to now there have been only a few cases where non expensive fillers have been used to prevent physical aging[17].

Here we report the use of a synthetic clay named saponite, to slow down the physical aging of PIM1 membranes. Saponite clays are phyllosilicates belonging to smectite family and can be easily prepared in laboratory through low-cost procedure[18].The synthetic clay is chosen as inexpensive and for the potential to improve the ageing behavior of the polymer due to its structure. The addition would affect the overall performance but the low loading explored combined with the starting very high permeability of PIM1 will still ensure a sufficient transport rate for application. However, given the inorganic nature of these materials it could be desirable to improve organic affinities via addition of organic moieties through functionalization processes. Addition in the interlayer space of suitable organic molecules are now well-known and can be carried out either using post-synthesis approaches[19,20,21] or by in using one-pot preparation step[22,23]. This latter method is generally considered as a less time consuming and should lead to a more homogenous dispersion of organic species on the clay surface, thus allowing to reduce the production costs.

In this work, two low-cost saponites samples (one completely inorganic and a second one functionalized with a surfactant) have been used as filler with PIM1 as polymeric matrix. Permeation performances of Mixed Matrix Membranes (MMMs) composed of PIM1 and saponite particles have been studied in the course of one year in order to explore physical aging effects over time. Interactions between the fillers and the polymeric matrix in addition to aging effects have been monitored through ss-NMR spectroscopy.

## EXPERIMENTAL SECTION

*Materials Preparation*

Synthesis of PIM1 was carried out by mixing anhydrous $K_2CO_3$ (11.05 g, 80 mmol), 5,5',6,6'-Tetrahydroxy-3,3,3',3'-tetramethyl-1,1'-spirobisindane (3.4 g, 10 mmol) and 2,3,5,6-Tetrafluoroterephthalonitrile (2.0 g, 10 mmol) in anhydrous dimethylformamide (65 mL) at

65°C for 72 h under $N_2$ atmosphere[24]. On cooling, the mixture was added to water (500 mL) and the crude product collected by filtration. Repeated precipitations from methanol gave 4.96 g (92% yield) of fluorescent yellow polymer (PIM1) with a Mw~87 000 $gmol^{-1}$. 3,3,3′,3′-Tetramethyl-1,1′-spirobiindane-5,5′,6,6′-tetraol and 2,3,5,6-tetrafluoro-phthalonitrile have been purified before use by recrystallization in methanol and ethanol respectively.

Ethanol and methanol were purchased from Fisher Chemicals. Anhydrous dimethylformamide (99.9%) and 5,5',6,6'-Tetrahydroxy-3,3,3',3'-tetramethyl-1,1'-spirobisindane (97%) were purchased from Alfa Aesar. Potassium Carbonate (99.5%) and 2,3,5,6-Tetrafluoroterephthalonitrile (98%) were purchased from Fluorochem.

Synthetic procedure for the preparation of clays, *i.e.* saponite and organo-modified saponite, was already established[18,23]. Here is reported only a brief summarization. Saponite synthesis gel with composition 1.0 $SiO_2$ : 0.835 MgO : 0.056 $Al_2O_3$ : 0.056 $Na_2O$ : 110 $H_2O$ was obtained from NaOH (>98 wt % Carlo Erba), $SiO_2$ ($SiO_2$ 99.8 wt %, Sigma Aldrich), $Mg(CH_3COO)_2{\cdot}4H_2O$ (>99%, Sigma Aldrich) and $Al[OCH(CH_3)_2]_3$ (>98%, Sigma Aldrich). The gel was poured in autoclave at 240 °C for 72 hours. The resulting material was then washed with deionized water until a neutral pH was reached and then dried at 80 °C for 24 hours. The sample is hereafter named SAP110, where 110 is the ratio between $H_2O$ and $SiO_2$ used for the preparation of the synthesis gel.

The hybrid organic-inorganic sample was prepared through a one-pot approach adapting a procedure already optimized in our laboratories that foresees the direct addition of hexadecyltrimethylammonium bromide (CTABr) to the reaction mixture[23]. In detail, to a synthesis gel with the same composition indicated above for the preparation of SAP110 sample, a quantity of CTABr (>98%, Sigma Aldrich) equal to twice the cation exchange capacity was added; the measured CEC of SAP110 was 59.7 mequiv/100 g. The gel was then put in autoclave at 200 °C K for 72 hours and then washed and dried. The resulting material is named SAP-OP.

*Membrane preparation*

Solution casting[25] at ambient conditions was used to fabricate dense film membranes with a filler content of 3 wt % (with respect of PIM1 weight). For the preparation of the membranes a suspension of filler (6 mg) in 5 mL $CHCl_3$ was sonicated with an ultrasound probe (Fisher Scientific, Model CL18, 120 W) for one hour, using a water bath to maintain the flask at room temperature. Meanwhile, 200 mg of PIM1 were dissolved in 5 mL of $CHCl_3$. After complete

dissolution, the PIM1 solution was added to the additive suspension with other 5 mL of $CHCl_3$. Then, the mixture was sonicated again for two hours at room temperature. The resulting solution was poured into a 5 cm glass petri dish. The membrane was allowed to form by slow solvent evaporation for 24-36 hours under a fume cupboard. Three membranes were obtained, namely a pure PIM1 membrane (PIM1), a MMM composed of PIM1 and SAP110 as a filler (PIM1-SAP110) and finally a MMM composed of PIM1 and SAP-OP (PIM1-SAP-OP). After the drying steps, the thickness of the membranes was determined with a digital micrometer (Mitutoyo). Before performing permeability measurements, the membranes were treated with methanol, by immersion in methanol for two hours, followed by a drying step under a fume cupboard for an hour and then under vacuum at room temperature overnight. It is well known that the permeability performances of PIM1 membranes may vary based on the casting conditions (for example, the choice of solvents) and the history of the sample. Alcohol washes away residual casting solvent and provides a comparable starting point for evaluation of different membranes.[25,26]

*Permeation measurements*

The permeation properties of the MMMs were tested using a constant volume - variable pressure method in an in-house built time-lag apparatus of which a schematic is reported in figure 1.

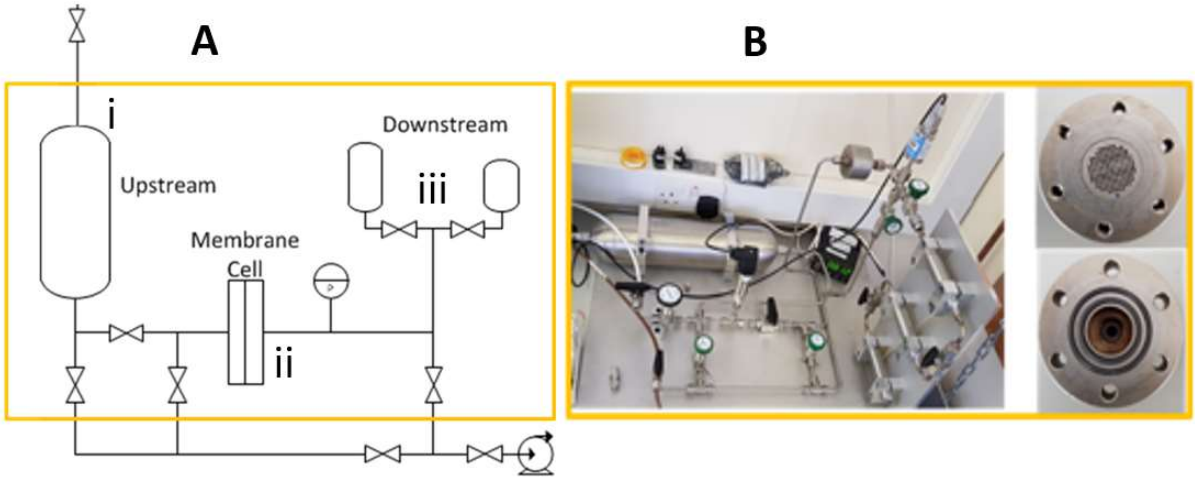


**Figure 1.** Permeation rig: (A) Schematic (B) Rig with the cell.

The permeation cell consists of three main parts, namely upstream, permeation cell and downstream. The upstream, or feed side, of the permeation cell consists of a controlling valve, a pressure gauge and a 2000 $cm^3$ volume gas reservoir. The sample is positioned in the gas permeation cell and sealed with two rubber O-rings. The downstream volume is fixed and a pressure transducer is used to detect pressure changes.

The permeability is obtained from the evolution of pressure of the downstream side (Brooks Transducer 1000 mBar, CMC Series). The permeability coefficient, *P*, was determined from the slope of the pressure vs. time curve under steady state condition (Equation 1).

$$P(G) = \frac{l}{A}\frac{V_{down}}{P_{up}RT}\left[\left(\frac{dP_{down}}{dt}\right)_{SS}\right] \quad \textbf{(Equation 1)}$$

Where l is the membrane thickness, A is the membrane area, $V_{down}$ is the downstream volume, $P_{up}$ is the upstream pressure, $P_{down}$ is the downstream pressure, T is the temperature recorded during analysis and R is the gas constant.
Before each experiment, the apparatus is vacuum-degassed and a leak rate is determined from the pressure increase in the downstream part.

The ideal selectivity between two gas species i and j is the ratio of the two single-gas permeabilities (Equation 2).

$$\alpha_{ij} = \frac{P(i)}{P(j)} \quad \textbf{(Equation 2)}$$

For the aging tests, the initial measurement is realised right after the methanol treatment. Then, the membrane is stored in a sealed plastic bag at ambient temperature and tested over time.

*Scanning Electron Microscopy*

The membranes have been examined with a JSM-IT100 (JEOL, Japan) operating at 10 kV. Before SEM analysis, the samples were fractured in liquid nitrogen and then sputtered with a layer of 9 nm gold to form a conductive surface.

*Thermogravimetric analysis*

Thermogravimetric analysis (TGA) was performed on a Setaram SETSYS Evolution instrument under argon (gas flow 20 mL/min), heating the samples up to 800 °C with a rate of 5 °C/min.

*XRD analysis*

X-ray diffraction (XRD) patterns were obtained on an ARL XTRA48 diffractometer using Cu KR radiation (λ =1.54062 Å) at r.t. between 2 and 65° 2θ with a step size of 0.02 with a rate of 1°2θ/min.

*Variable Temperature (VT) IR analysis*

VT-IR analyses were performed on a Fourier transform infrared (FTIR) Nicolet 5700 spectrometer (Thermo Optics) at a resolution of 4 $cm^{-1}$. The samples were pressed in the form of self- supporting wafers and placed into an IR cell equipped with KBr windows permanently attached to high vacuum line (residual pressure: $1.0*10^{-6}$ Torr, 1 Torr = 133.33 Pa). The experimental setup allowed all temperature treatments to be carried out in situ and in vacuum conditions. Spectra were collected by heating the samples from room temperature to 500 °C (heating rate of 10 °C/min) under vacuum conditions (residual pressure: $1.0*10^{-6}$ Torr, 1 Torr = 133.33 Pa).

*Transmission Electron Microscopy*

High-resolution transmission electron microscope micrographs (HRTEM) images were collected on a Zeiss libra200 FE3010 High Resolution Transmission Electron Microscope operating at 200 kV. The samples were encapsulated in sucrose (2.3 M) and then cut with a Cryoultramicrotome Reichert Jung with diamond knife.

*$N_2$ physisorption analysis*

Specific Surface Area analysis of Pure PIM and Saponite samples have been derived by $N_2$ physisorption measurements carried out at -196 °C and -186 °C, respectively. $N_2$ measurements were performed in the relative pressure range from $1 \times 10^{-6}$ to 1 $P/P_0$ by using a Quantachrome Autosorb 1MP/TCD instrument. Prior to the saponite samples analysis the samples were outgassed at 150 °C for 3 h (residual pressure lower than $10^{-6}$ Torr). PIM1 was treated at 120 °C overnight. Apparent surface areas were determined by using Brunauer-Emmett-Teller equation, in the relative pressure range from 0.01 to 0.1 $P/P_0$. Pore size distributions were obtained by applying both the NLDFT method ($N_2$ silica kernel based on a cylindrical pore

model applied to the desorption branch) and the classical BJH method applied to the desorption branch.

For the mixed matrix samples $CO_2$ equilibrium isotherms at 0 °C were measured using a novel Adsorption Differential Volumetric Apparatus, ADVA, custom built at the University of Edinburgh. Differently from conventional volumetric systems, the differential system relies on two symmetric branches, namely the sample and reference side, each comprising their dosing and uptake volume. The experiment is based on following the differential pressure between the sample side (where the sample is placed) and the reference side (where an inert material of the same sample volume is contained). The ADVA system is equipped with a 0 – 2 bar absolute pressure transducer and a +/- 621.3 mbar differential pressure transducer (Rosemount™ 3051 series). Four thermocouples are used to monitor the temperature of both dosing and uptake volumes in reference and sample side. Volumes of dosing and uptake cells are minimized to allow the use of very small amount of sample. For this study, both uptake cells were temperature controlled using a thermostatic bath. Prior the experiment, samples were regenerated in situ overnight at 35 °C. During regeneration, the sample is kept under vacuum using a high-vacuum turbomolecular pump (Pfeiffer HiCube 80 ECO - MVP 015-2).

*SS-NMR spectroscopy*

Solid-state NMR spectra were acquired on a Bruker Advance III 500 spectrometer and a wide bore 11.7 Tesla magnet with operational frequencies for $^{1}H$ and $^{13}C$ of 500.13 and 125.77 MHz, respectively. A 4 mm triple resonance probe in double resonance mode with MAS was employed in all the experiments. The as-cast polymer membranes were cut to small pieces so that it can be packed in a 4 mm Zirconia rotor and was spun at a MAS rate of 12 kHz. For the $^{13}C$ cross-polarization (CP) magic angle spinning (MAS) experiments, the proton radio frequencies (RF) of 55 and 28 kHz were used for initial excitation and decoupling, respectively. During the CP period the $^{1}H$ RF field was ramped using 100 increments, whereas the $^{13}C$ RF field was maintained at a constant level. During the acquisition, the protons were decoupled from the carbons by using a Spinal-64 decoupling scheme. A moderate ramped RF field of 55 kHz was used for spin locking, while the carbon RF field was matched to obtain optimal signal (40 kHz). T1 measurements were performed with a CPXT1 pulse sequence using a 10 ms spin-lock of 55 kHz and 40 kHz for $^{1}H$ and $^{13}C$, respectively, immediately followed by $\pi/2 - \tau - \pi/2$ sequence on $^{13}C$ with variable delay ($\tau$) ranging from 0.1 to 45 s. Spectra were recorded with a spectral width of 42 kHz and 256 transients were accumulated at 298 K. A line broadening of

50 Hz and zero filling to 2048 points were used. All chemical shifts are reported using δ scale and are externally referenced to TMS at 0 ppm. Data analysis were performed using Bruker software Dynamics Center, version 2.5.6 and T1 curves were obtained by plotting the intensity of the carbon signals versus time. A single exponential decay was used to fit the data using the equation 3:

$$I_t = I_0 e^{(-t/T_1)} \qquad \textbf{(Equation 3)}$$

## Results and Discussion

*Physico-chemical characterisation of saponite samples*

The XRD patterns of the saponite samples (both SAP110 and SAP-OP) are reported in Figure 2. XRD analysis of SAP110 (Fig. 2, a) shows three main reflections at 8°, 19.5° and 60.5° 2θ corresponding to (001), (110) and (060) planes, typical of the saponite structure[27]. The presence of the (060) reflection suggests that prepared clay has a trioctahedral structure[28]. The hybrid sample (SAP-OP) is characterised by the same XRPD reflections observed for SAP-110 (Fig. 2, b), suggesting that the hybrid sample prepared by the one-pot procedure in the presence of organic surfactant retains the structure typical of saponite clay. Nevertheless, a small shift towards lower angle of the basal (001) reflection (from 8° to 6.5° 2θ) is visible for SAP-OP respect to the fully inorganic sample. This fact indicates that SAP-OP has a more expanded interlayer space with respect to SAP-110 (the *d*-spacing for the two samples passes from 11 Å for SAP110 to 13.5 Å for SAP-OP) and it can be an indication of the presence of $CTA^+$ molecules between T-O-T sheets of SAP-OP[23]. Interlayer expansion upon $CTA^+$ functionalization was also encountered when intercalation, via one-pot approach, of $CTA^+$ species was conducted on saponite samples obtained with a $H_2O$/Si ratio of 20 (CTA-SAP_OP); distance between T-O-T sheets increased from 11, for the parent sample, to 13.5 Å for the functionalized sample[23]. These studies indicated that $CTA^+$ species are arranged parallel to saponite lamellae, according to the low charge density of the saponite sample[23]. In the context of the present study very similar interlayer distances are found for the pristine and hybrid clays. Given the dimension of $CTA^+$ molecule and the similarity of the system under study to that of CTA-SAP_OP, it is reasonable to assume a similar configuration for the surfactant molecules in the case of SAP-OP sample.

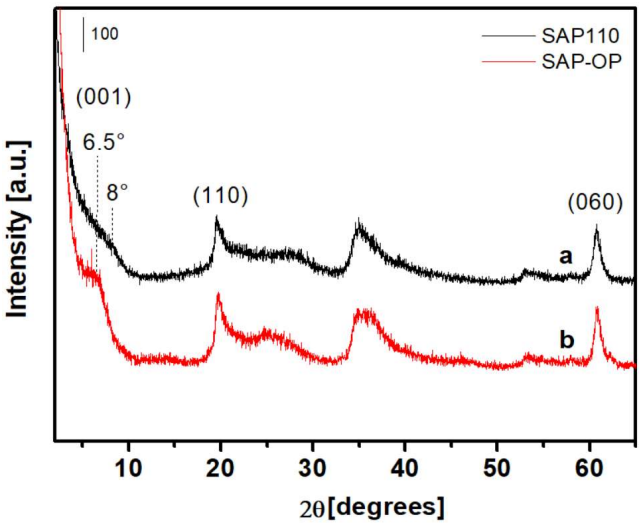


**Figure 2.** XRD pattern of SAP110 (a) and SAP-OP (b) samples.

Thermogravimetric analysis of SAP110 and SAP-OP samples are reported in Figure 3A. From the comparison of TGA (Fig. S1 in the Supporting Information) and DTG data (Figure 3A) collected for pristine SAP-110 and hybrid derived sample, it can be noticed that the SAP-OP contains a lower amount of adsorbed water molecules with respect to pure saponite sample (Figure 3A, curve a), as witnessed by the lower weight losses at *ca*. 100 °C (1.7 wt % for SAP-OP vs *ca.* 6 wt % for SAP-110). This behavior suggested that the intercalation of $CTA^+$ ions modifies the hydrophilic character of the saponite interlayer, as also observed in the literature[23]. Moreover, the hybrid samples displayed an evident weight loss in the 250°C-500°C, totally absent for SAP-110, assigned to the CTA decomposition[23]. From thermogravimetric analysis it was possible to derive the amount of $CTA^+$, which is assessed at 6.3 wt %. This was also confirmed by CHN analysis (Table S1 in the Supporting Information).

The presence of surfactant molecules in SAP-OP and the corresponding thermal degradation behavior were also studied by using IR analysis at variable temperature (VT-IR, Fig. 3B). VT-IR spectra were recorded from room temperature (rt) to 500 °C.

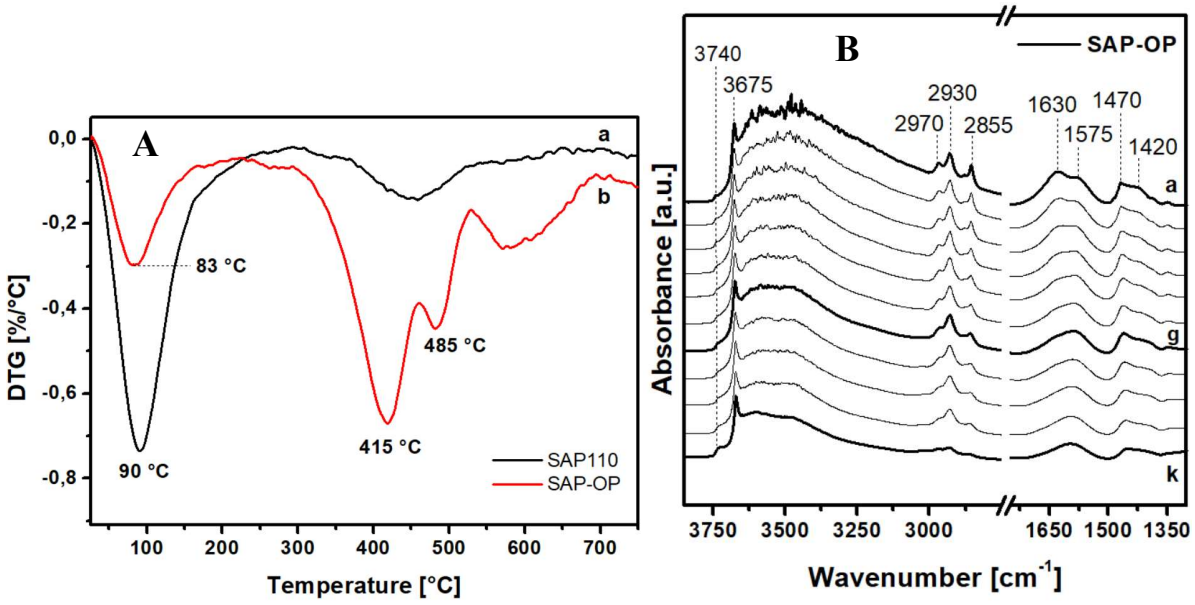


**Figure 3.** (A) Differential TG curves (DTG) curves of SAP110 (a) and SAP-OP (b) collected under Ar flow (20 mL/min) from 25 to 800 °C. (B) IR spectra of SAP-OP collected at variable temperature. Spectra are recorded at room temperature (a), at 50 °C (b) and from (b) to (k) every 50 °C up to 500°C (k).

The IR spectrum collected at rt (Figure 3B, a) is characterized by the presence of a sharp band at 3670 $cm^{-1}$ and a broad band in the 3600-3400 $cm^{-1}$ range. Moreover, bands at 2970, 2930 and 2855 $cm^{-1}$ are also visible, together with bands in the 1650-1300 $cm^{-1}$ range. The assignment of the IR absorption bands of SAP-OP at rt are reported in Table 1.

| Bands position [$cm^{-1}$] | Assignments |
|---|---|
| 3740 | ν [Si]-O-H |
| 3675 | ν O-H (octahedral Mg) |
| 3600 - 3450 | ν O-H physisorbed water |
| 2970 | $\nu_{as}$ Aliphatic C-H (-$CH_3$) |
| 2930 | $\nu_{as}$ Aliphatic C-H (-$CH_2$-) |
| 2855 | $\nu_s$ Aliphatic C-H (-$CH_2$-) |
| 1630 | δ O-H physisorbed water |
| 1500 - 1300 | δ Aliphatic C-H (-$CH_2$-, -$CH_3$) |

**Table 1.** Assignments of the main IR vibrations of SAP-OP from [23].

Upon heating the sample up to 300 °C and by comparing the corresponding IR spectrum (Fig. 3B, g) to the spectrum at r.t. (Fig. 3B, a) the desorption of physisorbed water is observed, as evidenced by the decrease in the intensity of the broad band in the 3600-3000 $cm^{-1}$ region in addition to the diminishing of the band at 1630 $cm^{-1}$.

Thermal treatment up to 300 °C did not affect the organic species as it is also evidenced by thermogravimetric analysis reported in Figure 3 (A). Thermal degradation of $CTA^+$ species is found to occur between 400 and 500 °C through the decrease in intensity of the signals found in the 2970 - 2855 and 1500-1300 $cm^{-1}$ regions, respectively associated with stretching modes and bending modes of $-CH_2-$ and $-CH_3$ groups. Removal of $CTA^+$ during thermal treatment cause the appearance of a new band at 3740 $cm^{-1}$ due to isolated silanol species on the saponite surface[23]. This band was not observed in the presence of $CTA^+$ species because of the interaction of the surface Si-OH groups with surfactant molecules. Thermal treatment up to 500 °C did not seem to affect the integrity of the saponite framework, as it is evidenced by the presence of the signal at 3675 $cm^{-1}$ (Figure 3B, curve k) associated with magnesium octahedral species. The presence of a weak broad band around 1630 $cm^{-1}$ after the thermal treatment is due to the Si-O-Si vibration of the saponite framework[23].

*Membrane characterization and permeability measurements*

The Mixed Matrix Membranes (MMMs) obtained by adding saponite clays to the polymeric matrix PIM1 appear homogenous at macroscopic scale (Fig. S3 in the Supporting Information). A more in-depth analysis has been carried out by means of Scanning Electron Microscopy (Fig. 4). Saponite particles appear well dispersed within the polymeric matrix for both samples. Nevertheless, particles dimension is heterogeneous, ranging from few hundreds nanometres to micron size. The rough surface of the samples (e.g. PIM1-SAP110) is the result of the cutting process to obtain the cross section.

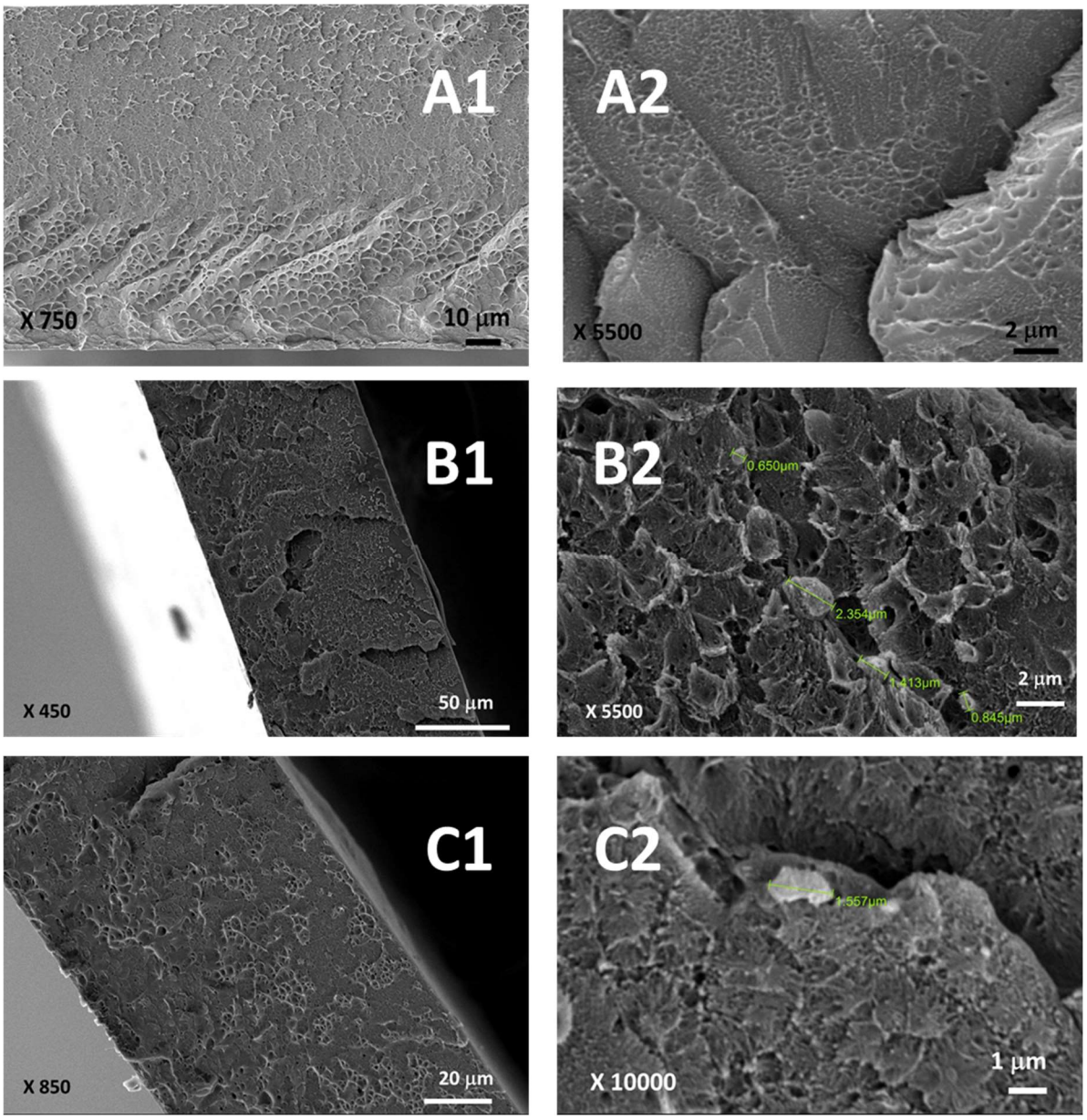


**Figure 4**. SEM images of membrane samples of pure PIM1 (A) and MMMs, PIM1-SAP110 (B) and PIM1-SAP-OP (C) (at two magnifications).

TEM analysis of PIM1-SAP-OP sample is reported in Figure 5. The presence of saponite aggregates was also evidenced by TEM, showing tactoids of sheet-like crystals. Nevertheless, in some cases, aggregates of few layers are also evidenced (see Fig. 5B)[17].

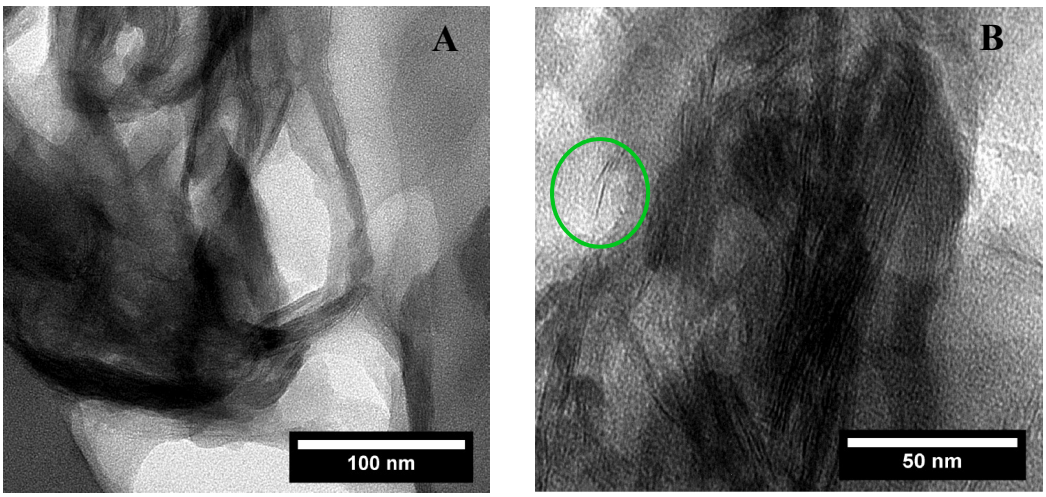


**Figure 5.** TEM micrographs of a section of PIM1-SAP-OP sample at different magnifications.

XRD patterns of both pure PIM1 aged membrane sample and aged MMMs are reported in Figure S4. Pure PIM1 XRD pattern reveals the classical reflections associated with the amorphous nature of the polymer. The broad band around 23° 2θ is typical of aromatic systems [29], the second band around 18° 2θ is related to the chain to chain distance of efficiently packed polymeric chains, also related to the presence of ultra-micropores[29]. The band around 13° 2θ is probably due to the fraction of inefficiently packed polymeric chains[29]. When saponite particles are introduced a small shift toward higher 2θ values, hence smaller inter-chain spacing, is seen. This can be attributed to enhanced packing of polymeric chains.

In order to test physical aging effects on MMMs, permeability measurements were performed right after MeOH treatment and at later times, up to approximately one year. Table 2 shows permeation measurement results for PIM1 and MMMs after MeOH treatment ($t_0$).

| Separation performance @ $t_0$ (MeOH treatment) | Permeability $CO_2$ [Barrer] (+/- 5%) | Selectivity $CO_2/N_2$ (+/- 9%) |
|---|---|---|
| PIM1 | 13400 | 15 |
| PIM-SAP110 | 12300 | 16 |
| PIM-SAP-OP | 10200 | 15 |

**Table 2:** Permeation data for PIM1, PIM-SAP110 and PIM-SAP-OP at $t_0$ (MeOH treatment). [1 Barrer = $10^{-10}$ $cm^3$ (STP)·cm·$cm^{-2}$·$s^{-1}$·$cmHg^{-1}$].

$CO_2$ permeation data of PIM1 are in the range found in literature (around 12000-13000 Barrer)[26,30].

By adding saponite fillers, the $CO_2$ permeability decreases by 8% and 24% for PIM1-SAP110 and PIM1-SAP-OP, respectively. The $CO_2/N_2$ selectivity remains unchanged at $t_0$ for the PIM-SAP-OP respect to PIM1 membrane while a slight increase is observed for PIM-SAP110 membrane. It is worth noting that saponite fillers possess lower specific surface area with respect to PIM1. Indeed, PIM1 shows SSA of 790 $m^2/g$ whereas the saponite samples are characterized by a lower SSA of 230 $m^2/g$ and 300 $m^2/g$ for SAP-OP and SAP110, respectively. Pore size distributions of SAP-OP and SAP110 samples are reported in figure S2 in the Supporting Information. The addition of saponite samples to PIM1 polymer results in lower surface area for the MMMs at $t_0$, with respect to the parent membrane that correlates with the lower solubility of the gas species in the matrix and therefore a lower permeability. MMMs surface areas were also measured for the one-year aged samples and data are reported in Table 2. Both PIM1-SAP110 and PIM1-SAP-OP show a similar decrease in surface area compared to the original polymer consistent with the lower surface area of the additives.

| Sample | $SSA_{BET}$ [$m^2/g$] |
|---|---|
| **PIM1**[a] | 790 |
| **PIM1 - SAP110**[b] | 535 |
| **PIM1 - SAP-OP**[b] | 486 |

**Table 2.** Specific Surface Area (SSA) **a**) obtained from $N_2$ physisorption at -196.15 °C and **b**) obtained from $CO_2$ physisorption at 0 °C. $CO_2$ uptake curves are shown in Fig. S5 in the Supporting Information.

In Figure 6, normalized permeation data are reported as a function of aging. Permeability measurements were conducted in the course of approximately one year. Measurements are performed after leaving the sample under vacuum over-night at room temperature.

Aging effects on all samples are clearly visible in the first few days after methanol treatment. PIM1 displays the classical aging behaviour exhibited by Polymers of Intrinsic Microporosity[31], namely a progressive drop in the permeation capacity associated with both $CO_2$ and $N_2$ caused by the collapse of free volume[26,32]. After 315 days $CO_2$ permeability of pure PIM1 is 21% of the original $t_0$ value, while for $N_2$ the value is 15% of the initial permeability, hence an increase in selectivity over time towards $CO_2$ is observed. This is consistent with other studies in the literature that recorded an increase in selectivity after ageing of PIM1[12,15].

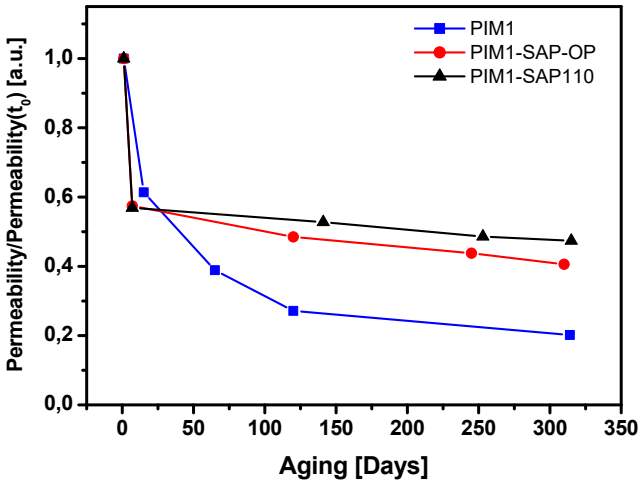


**Figure 6.** Normalized $CO_2$ permeability data with respect to $t_0$ values of PIM1 (■), PIM-SAP-OP (●) and PIM-SAP110 (▲) as function of time. Lines are drawn to guide eye. Estimated error on permeability is +/- 5% and on selectivity is +/- 9%.

As shown in Figure 6, the addition of saponite fillers results in a drastic drop in $CO_2$ permeability within the first 7 days after membranes regeneration in MeOH. For both MMMs the initial drop is of 43% with respect to $t_0$ value. After 7 days a significative reduction in the slope of both MMMs curves is seen. This effect is not seen for the data associated with PIM1. Up to approximately 320 days after MeOH treatment the value of the $CO_2$ permeability for

PIM-SAP110 membrane is 47% with respect to $t_0$ values, while for PIM-SAP-OP is 41%. One possible explanation for the slight divergence in aging performances between MMMs can be associated with intercalation of PIM1 polymeric chains within saponite's interlayer. A similar phenomenon was also encountered in the context of MMMs systems composed of PIM1 and Porous Aromatic Frameworks (PAF), where bulky moieties of PIM1 were found to penetrate inside PAF pores, thus allowing the preservation of small free volumes, hence reducing aging effects[12,15]. For SAP110, without organic molecules between T-O-T sheets, PIM1 polymeric chains can be accommodated in the interlayer space, to a certain extent; in this situation, the chains are confined and restricted from further movements, thus resulting in decreased aging rate. In the case of SAP-OP, the interlayer space is partially occupied by $CTA^+$ organic chains. This could somewhat impede the diffusion of a fraction of PIM1 polymeric chains within T-O-T sheets. The initial strategy in adopting an inorganic – organic hybrid material as a membrane filler, was to exploit favorable interactions between similar species, namely an organic matrix with an intercalated surfactant. However, for the system under study, it seems that allowing chains diffusion between the filler sheets is a more effective way to slow down PIM1 physical aging. It is interesting that a decrease in aging rate is achieved with a filler content of only 3 wt %, while it is observed that higher contents of fillers possessing much higher SSA like MIL-101 do not necessarily lead to slower aging rates of PIM1 matrix[13].

In terms of separation performances, physical aging often results in increase in the selectivity[15] toward $CO_2$ over $N_2$ as reported in literature. After 1 year of aging $CO_2/N_2$ selectivity for the pure PIM1 membrane is increased from 15 to 19 while for PIM1-SAP110 membrane from 16 to 17 and from 15 to 22 for PIM1- SAP-OP membrane.

*Monitoring the interactions between saponite samples and PIM1 by SS-NMR analysis*

As reported in the literature, molecular level dynamics in polymer membranes can be monitored by employing solid-state NMR spectroscopy (SS-NMR) and $^{13}C$ spin–lattice relaxation times (T1) measurements, which can give an indication of aging in glassy polymers[12]. The $^{13}C$ relaxation studies allow one to estimate the variation in the degree of flexibility of the polymer as it undergoes ageing. As of today, to our knowledge, monitoring of aging processes in PIM1 membranes through SS-NMR spectroscopy has only appeared in few studies[12,15]. The $^{13}C$ NMR spectra for the three membrane samples, PIM1, PIM1-SAP110 and PIM1-SAP-OP are shown in Figure 7(A).

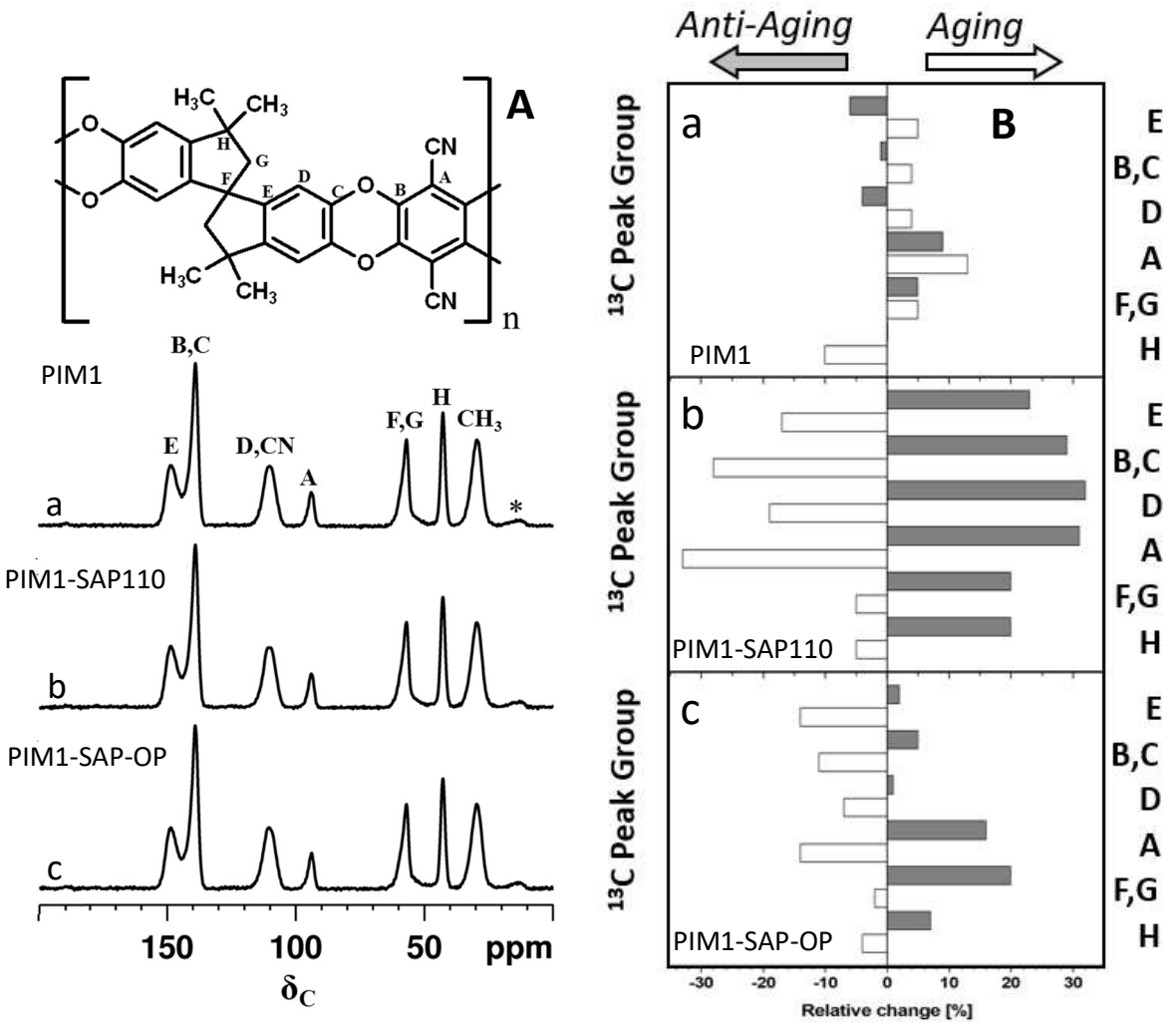


**Figure 7**: Frame A:[13]C CPMAS NMR spectra of various PIM1 based membranes: a) PIM1, b) PIM1-SAP110 and c) PIM1-SAP-OP. Spectra were recorded using a MAS rate of 12 kHz and a CP contact time of 10 ms; * denotes spinning sidebands. Frame B) bar charts representing percentage changes in T1 relaxation times of chemical groups assigned in figure 7 (A) between $t_3$ (3 months aging) and $t_0$ (MeOH treatment) ■, while □ represents percentage changes between $t_{12}$ (one-year aging) and $t_3$.

The [13]C resonances are broad as a result of restricted mobility due to rigidity of the polymer, make it difficult to derive additional information. The resolution and intensities, however, are ample for the measurement of relaxation times and chemical shifts which would give additional information Assignment of ss-NMR resonance peaks are reported in Figure 7 (A), following data appeared in the literature[12,15].

The magnitude of the influence of additives on the individual carbons of PIM1 appears to be limited as no apparent change in the $^{13}C$ chemical shift values and peak resolution were observed for MMMs with respect to the pure PIM1 sample.

The $^{13}C$ spin–lattice relaxation time (T1) measurements can reveal the specific nature and influence of additives on the molecular level dynamics in polymer membranes. $^{13}C$ relaxation studies allow to estimate the aging in polymer membranes as the T1 values are related to the mobility/rigidity of specific carbon atoms within the polymer. To investigate further, the $^{13}C$ T1 values at ambient temperature were measured for the three samples (Table S1 in the Supporting Information).

T1 values were obtained at three different times, namely right after MeOH treatment ($t_0$), after 3 months ($t_3$) and after almost 12 months of aging ($t_{12}$). Relative changes in the T1 value of PIM1 membranes are shown in Figure 7(B). Relative rate of change of $^{13}C$ spin–lattice relaxation times have been evaluated using the formula $[(t_{final} - t_{initial})/t_{initial}]$; changes in T1 values were evaluated for the first 3 months by means of the formula $[(t_3-t_0)/t_0]$, while from 3 months to 12 months the formula $[(t_{12}-t_3)/t_3]$ was used.

In the MeOH treated pure PIM1 membrane, the methyl carbons which resonate at around 30 ppm, relax rapidly (T1 of the order of milliseconds), whereas the other carbons have relatively long relaxation times (T1 of the order of seconds). The methyl carbons are therefore in a highly mobile state while the backbone chain segments are rigid. As aging occurs, from $t_0$ to $t_3$, it is observed an increase in the T1 values for carbons A and F while for other carbons a decrease in T1 values was found. Aging in the second period, namely from 3 to 12 months, also shows that almost all of PIM1 carbons (except H) have longer $T_1$ values. These results show that as the polymer membrane ages, the relaxation times of polymer carbons increase as the chain mobility decreases. Previous studies on PIM1 have also reported similar changes in $T_1$ values[12,15]. When free volume inside the PIM1 membrane is reduced, carbon mobility is reduced and longer T1 are observed[15].

In the case of PIM1-SAP110 composite, uniformly higher T1 values were recorded for all carbons in the first three months period. This reflects a decrease in free volume, as consequence of polymer chains densification with respect to $t_0$ sample. Increase in chains densification results in lower permeation pathways for gas molecules. Indeed, the overall $CO_2$ permeability of PIM1-SAP110 displayed a drop in the first week and then only small additional drop up to three months, as was evidenced by permeability measurements (Figure 6). However,

comparing T1 values at three months to T1 values after almost one year, a decrease for all carbons in $^{13}C$ spin–lattice relaxation times can be observed. This reduction in the spin-lattice relaxation times is due to greater molecular mobility of the polymer backbones as a result of their favourable interactions with saponite. Chains intercalation between T-O-T sheets could result in the preservation of small free volumes thus resulting in lower T1 values.

Although the partial collapse of the free volume in PIM1-SAP110 cannot be ruled out, the presence of clay particles, does not allow further densification of PIM1 chains. A possible explanation could be that while portions of PIM1 chains diffuse within T-O-T sheets, they experience a less crowded environment which acts as additional free volume. Physical aging is thus diminished on the longer-term in saponite based composites as a consequence of chains confinement, which result in less packed polymeric chains.

A similar trend was also observed for PIM1-SAP-OP. The increase in the $^{13}C$ spin–lattice relaxation times in the first three months period is related to the decrease in free volume caused by the densification of polymer chains. However, the $^{13}C$ $T_1$ values decrease between three and twelve months evidencing the influence of SAP-OP incorporation on the polymer relaxation rate. Overall, PIM1-SAP-OP behaves similarly to PIM1-SAP110, however between $t_3$ and $t_{12}$, SAP-OP seems less effective in decreasing T1 values, which is reflected in faster aging with respect to SAP110, as was evidenced by permeability measurements. Interlayer functionalization of SAP-OP could result in lower PIM1 chains diffusion; hence less free volume is retained.

The rate of change of $T_1$ values appeared to be dependent on the nature of the carbons as aromatic units were influenced strongly. The layered structure of saponite enforces the intrusion of polymer chains into interlayer space leading to the mobility of the longer segments of backbone chains which results in free volume. Consequently, physical aging at long-term in PIM1 is moderated by the presence of saponite.

## Conclusions

Mixed Matrix Membranes (MMMs) composed of PIM1 and synthetic clays as additives were prepared by solution casting at ambient conditions. Synthetic clays were obtained using a $H_2O$/Si ratio of 110 in order to prepare a clay with nanosized dimension. A completely inorganic material, SAP110, and an inorganic-organic hybrid sample prepared by one-pot

procedure, SAP-OP, have been prepared. XRD analysis revealed the crystalline and layered nature of saponites; it was found that functionalization led to an increase in spacing between T-O-T sheets, from 11 Å of SAP-110 to 13.5 Å of SAP-OP. From TGA analysis it was seen that $CTA^+$ found in SAP-OP showed higher thermal stability with respect to pure CTABr. This suggests that $CTA^+$ species are found between T-O-T sheets which results in a protective effect.

The decomposition process of $CTA^+$ species of SAP-OP sample was further studied by VT-IR analysis in agreement with TGA findings.

$CO_2$ and $N_2$ permeability measurements were carried out for a period of more than 300 days in order to study aging effects on MMMs as well as on pure PIM1 membrane which was used as a reference sample. PIM1 exhibits the classical aging behaviour of polymers of intrinsic microporosity, namely a progressive decline in gas permeation due to reduction in internal free volume caused by polymeric chains mobility.

Both PIM1-SAP110 and PIM1-SAP-OP present an initial significant drop of 43% in $CO_2$ permeability up to 7 days. However, from 7 days up to approximately one-year, further loss in $CO_2$ permeability is assessed at 10 and 16% for PIM-SAP110 and PIM-SAP-OP respectively. This indicates that saponite fillers can effectively slow down aging of PIM1 membranes in the long term. Differences in performances between saponite fillers are probably due to lower ability of SAP-OP to accommodate PIM1 chains between T-O-T sheets due to the presence of $CTA^+$ species.

The $CO_2/N_2$ selectivity of all three membrane samples was found to increase; for the pure PIM1 membrane from 15 to 19, for PIM1-SAP110 from 16 to 17 and from 15 to 22 for PIM1- SAP-OP membrane.

SS-NMR spectroscopy was used to study MMMs and PIM1 membrane aging effects through $^{13}C$ spin–lattice relaxation times (T1), which allow the study of molecular level dynamics. T1 values were recorded right after MeOH treatment ($t_0$), after three months of MeOH treatment ($t_3$) and after twelve months of MeOH treatment ($t_{12}$). T1 values for almost all carbons were found to increase for PIM1 in a twelve months period, thus indicating chains compaction and consequently a progressive aging. For MMMs higher T1 values were found after three months for all carbons thus indicating a rapid aging. However, a decrease in T1 values were found by comparing $t_{12}$ with $t_3$. Shorter T1 values are symptomatic of higher mobility of the corresponding carbons and consequently this is an indication of slower aging for the PIM1 matrix. PIM1 chains intercalation between the saponite sheets could be one of the mechanisms

responsible. Diffusion of polymeric chains could result in the preservation of small free volumes thus producing lower T1 values.

This is consistent with permeability measurements findings. PIM1-SAP-OP exhibits the same behaviour of PIM-SAP110 up to three months, however a less evident decrease in T1 values was found between $t_3$ and $t_{12}$. This indicates a weaker effect in slowing physical aging for SAP-OP. PIM1 intercalation could be somewhat prevented for SAP-OP because of interlayer functionalization. This is also consistent with permeability measurements findings which give a lower permeability for PIM1-SAP-OP at $t_{12}$ of 7% with respect to PIM1-SAP110.

Saponite clays as PIM1 additives shows the ability of slowing aging effects in PIM1 membranes. Chains confinement between lamellar sheets could play a significant role in reducing chains densification, while maintaining small free volumes.

## Associated Content

## Supporting Information

The Supporting Information is available free of charge at https://pubs.acs.org/

Thermogravimetric analysis of SAP110 and SAP-OP samples, pore size distribution of SAP110 and SAP-OP samples, images of PIM1 and MMMS, XRD pattern of pristine aged PIM1 membrane sample, aged PIM1-SAP110 and aged PIM1-SAP-OP, $CO_2$ adsorption isotherms acquired at 0 °C for MMMs. CHN analysis of SAP-OP sample, $^{13}C$ Spin-lattice relaxation times ($T_1$) of PIM1 and MMMs.

## Acknowledgements

C. B. and G. G. thank Dr. Marcello Marelli (CNR-SCITEC, Italy) and Dr. Simone Cantamessa (Università del Piemonte Orientale, Italy) for TEM measurements.

M.C.F. has received funding from the EPSRC (UK) grant number EP/R000468/1.

## References


[1] Abanades, J.C.; Arias, B.; Lyngfelt, A.; Mattisson, T.; Wiley, D.E.; Li, H.; Ho, M.T.; Mangano, E.; Brandani, S.; Emerging $CO_2$ Capture Systems. Int. J. Greenhouse Gas Control. 2015, 40, 126-166.

[2] Peters, L.; Hussain, A.; Follmann, M.; Melin, T.; Hägg. M.B.; $CO_2$ Removal from Natural Gas by employing amine absorption and membrane technology - A technical and economical analysis. Chem. Eng. J. 2011, 172, 952– 960.

[3] Chabanon, E.; Bounaceur R.; Castel, C.; Rode, S.; Roizard, D.; Favre. E.; Pushing the limits of intensified $CO_2$ post-combustion capture by gas–liquid absorption through a membrane contactor. Chem. Eng. Process. 2015, 91, 7–22.

[4] Stern, S. A.; Polymers for gas separations: the next decade. J. Membr. Sci. 1994, 94, l-65.

[5] McKeown, N. B.; Makhseeda, S.; Budd. P. M.; Phthalocyanine-based nanoporous network polymers. Chem. Commun. 2002, 23, 2780 –2781.

[6] McKeown, N. B.; Budd, P. M.; Msayib. K. J.; Ghanem, B. S.; Kingston, H. J.; Tattershall, C. E.; Makhseed, S.; Reynolds, K. J.; Fritsch. D.; Polymers of Intrinsic Microporosity (PIMs): Bridging the Void between Microporous and Polymeric Materials. Chem. - Eur. J. 2005, 11, 2610–2620.

[7] Budd, P. M. Ghanem, B. S.; Makhseed, S.; McKeown, N. B.; Msayib K. J.; Carin E. Tattershall, C. E.; Polymers of intrinsic microporosity (PIMs): robust, solution-processable, organic nanoporous materials Chem. Commun., 2004, 230–231.

[8] Tiwari, R. R.; Jin, J.; Freeman, B.D.; Paul, D.R.; Physical aging, $CO_2$ sorption and plasticization in thin films of polymer with intrinsic microporosity (PIM-1). J. Membr. Sci. 2017, 537, 362–371.

[9] Bernardo, P.; Bazzarelli, F.; Tasselli, F.; Clarizia, G.; Mason, C. R.; Maynard-Atem, L.; Budd, M.; Lanč, M.; Pilnáček, K.; Vopička, O.; Friess, K.; Fritsch, D.; Yampolskii, Y. P.; Shantarovich, V.; Jansen, J. C.; Effect of physical aging on the gas transport and sorption in PIM-1 membranes. Polymer. 2017, 113, 283 – 294.

[10] Mitra, T.; Bhavsar, R. S.; Adams, D. J.; Budd P. M.; Cooper, A. I.; PIM-1 mixed matrix membranes for gas separations using cost-effective hypercrosslinked nanoparticle fillers. Chem. Commun. 2016, 52, 5581-5584.

[11] Kinoshita, Y.; Wakimoto, K.; Gibbons, A. H.; Isfahani, A. P.; Kusuda, H.; Sivaniah, E.; Ghalei, B.; Enhanced PIM-1 membrane gas separation selectivity through efficient dispersion of functionalized POSS fillers. J. Membr. Sci. 2017, 539, 178-186.

[12] Lau, C.H.; Konstas, K.; Thornton, A.W.; Liu, A.C.Y.; Mudie, S.; Kennedy, D.F.; Howard, S.C.; Hill, A.J.; Hill, M.R.; Gas-Separation Membranes Loaded with Porous Aromatic Frameworks that Improve with Age., Angew. Chem. Int. Ed. 2015, 54, 2669 –2673.

[13] Khdhayyer, M; Bushell, A. F.; Budd, P.M.; Attfield, M. P.; Jiang, D.; Burrows, A. D.; Esposito, E.; Bernardo, P.; Monteleone, M. Fuoco, A.; Clarizia, G.; Bazzarelli, F.; Gordano, A.; Jansen, J. C.; Mixed matrix membranes based on MIL-101 metal–organic frameworks in polymer of intrinsic microporosity PIM-1. Sep. Purif. Technol. 2019, 212, 545-554.

[14] Alberto, M.; Bhavsar, R.; Luque-Alled, J. M.; Vijayaraghavan, A.; Budd P. M.; Gorgojo, P.; Impeded physical aging in PIM-1 membranes containing graphene-like fillers. J. Membr. Sci. 2018, 563, 513-520.

[15] Lau, C. H.; Nguyen, P. T.; Hill, M. R.; Thornton, A. W.; Konstas, K.; Doherty, C. M.; Mulder, R. J.; Bourgeois, L.; Liu, A. C. Y.; Sprouster, D. J.; Sullivan, J. P.; Bastow, T. J.; Hill, A. J.; Gin, D. L.; Noble, R. D.; Ending Aging in Super Glassy Polymer Membranes, Angew. Chem. Int. Ed. 2014, 53, 5322 –5326.

[16] Smith, S. J. D.; Hou, R.; Konstas, K.; Akram, A.; Cher Hon Lau, C. H.; R. Hill, M. R.; Control of Physical Aging in Super-Glassy Polymer Mixed Matrix Membranes. Acc. Chem. Res. doi.org/10.1021/acs.accounts.0c00256.

[17] Hou, R.; Smith, S. J. D.; Wood, C. D.; Roger J. Mulder, R. J.; Lau, C. H.; Wang, H.; Hill, M. R.; Solvation Effects on the Permeation and Aging Performance of PIM-1-Based MMMs for Gas Separation. ACS Appl. Mater. Interfaces. 2019, 11, 6502−6511.

[18] Costenaro, D.; Gatti, G.; Carniato, F.; Paul, G.; Bisio, C.; Marchese, L.; The effect of synthesis gel dilution on the physico chemical properties of acid saponite clays. Microporous Mesoporous Mater. 2012, 162, 159–167.

[19] Kooli, F.; Khimyak, Y. Z.; Alshahateet, S. F.; Chen, F.; Effect of the Acid Activation Levels of Montmorillonite Clay on the Cetyltrimethylammonium Cations Adsorption. Langmuir. 2005, 21, 8717-8723.

[20] He, H.; Frost, R. L.; Bostrom, T.; Yuan, P.; Duong, L.; Yang, D.; Xi, Y.; Kloprogge, J. T.; Changes in the morphology of organoclays with $HDTMA^+$ surfactant loading. Appl. Clay Sci. 2006, 31, 262–271.

[21] Richard-Plouet, M.; Vilminot, S.; Guillot, M.; Synthetic transition metal phyllosilicates and organic-inorganic related phases. New J. Chem., 2004, 28, 1073–1082.

[22] Jaber, M.; Miehe´-Brendle´, J.; Synthesis, characterization and applications of 2:1 phyllosilicates and organophyllosilicates: Contribution of fluoride to study the octahedral sheet. Microporous Mesoporous Mater. 2008, 107, 121–127.

[23] Bisio, C.; Carniato, F.; Paul, G.; Gatti, G.; Boccaleri, E.; Marchese, L.; One-Pot Synthesis and Physicochemical Properties of an Organo-Modified Saponite Clay. Langmuir. 2011, 27, 7250–7257.

[24] Merkel, T. C.; Bondar, V.; Nagai, K.; Freeman, B. D.; Sorption and Transport of Hydrocarbon and Perfluorocarbon Gases in Poly(1-trimethylsilyl-1-propyne). J. Polym. Sci., Part B: Polym. Phys. 2000, 38, 273–296.

[25] Budd, P. M.; Elabas, E. S.; Ghanem, B. S.; Makhseed, S.; McKeown, N. B.; Msayib, K. J.; Tattershall, C. E.; Wang, D.; Solution processed, organophilic membrane derived from a polymer of intrinsic microporosity. Adv.Mater. 2004, 16, 456–459.

[26] Budd, P. M.; McKeown, N. B.; Ghanem, B. S.; Msayib, K. J.; Fritsch, D.; Starannikova, L.; Belov, N.; Sanfirova, O.; Yampolskii, Y.; Shantarovich. V.; Gas permeation parameters and other physicochemical properties of a polymer of intrinsic microporosity: Polybenzodioxane PIM-1. J. Membr. Sci. 2008, 325, 851–860.

[27] Bisio, C.; Gatti, G.; Boccaleri, E.; Marchese, L.; Bertinetti, L.; Coluccia, S.; On the Acidity of Saponite Materials: A Combined HRTEM, FTIR, and Solid-State NMR Study. Langmuir 2008, 24, 2808-2819.

[28] Prihod'ko, R.; Hensen, E. J. M.; Sychev, M.; Stolyarova, I.; Shubina, T. E.; Astrelin, I.; van Santen, R. A.; Physicochemical and catalytic characterization of non-hydrothermally

synthesized Mg-, Niand Mg–Ni-saponite-like materials. Microporous Mesoporous Mater. 2004. 69, 49–63.

[29] Yong, W. F.; Li, F. Y.; Chung, T-S.; Yen Wah Tong, Y. W.; Highly Permeable Chemically Modified PIM-1/Matrimid Membranes for Green Hydrogen Purification. J. Name., 2013, 00, 1-3.

[30] McKeown, N. B.; Budd, P. M.; Polymers of intrinsic microporosity (PIMs): organic materials for membrane separations, heterogeneous catalysis and hydrogen storage. Chem. Soc. Rev., 2006, 35, 675–683.

[31] Swaidan, R.; Ghanem, B.; Litwiller, E.; Pinnau, I. Physical Aging, Plasticization and Their Effects on Gas Permeation in “Rigid” Polymers of Intrinsic Microporosity, Macromolecules. 2015, 48, 6553−6561.

[32] Harms, S.; Rätzke, K.; Faupel, F.; Chaukura, N.; Budd, P. M.; Egger, W.; Ravelli. L.; Aging and Free Volume in a Polymer of Intrinsic Microporosity (PIM-1). The Journal of Adhesion. 2012, 88, 608-619.